========= **PRODUCTION, STRUCTURE, PROPERTIES** =========

Effect of CrB₂ on the Microstructure, Properties, and Wear Resistance of Sintered Composite and the Diamond Retention in Fe−Cu−Ni−Sn Matrix

V. A. Mechnik[a] *, N. A. Bondarenko[a], V. M. Kolodnitskyi[a] **, V. I. Zakiev[b], I. M. Zakiev[b], E. S. Gevorkyan[c], V. A. Chishkala[d], and N. O. Kuzin[e]

[a] *Bakul Institute for Superhard Materials, National Academy of Sciences of Ukraine, Kyiv, 04074 Ukraine*
[b] *National Aviation University, Kyiv, 03068 Ukraine*
[c] *Ukrainian State University of Railway Transport, Kharkiv, 61001 Ukraine*
[d] *Karazin Kharkiv National University, Kharkiv, 61022 Ukraine*
[e] *Lazaryan National University of Railway Transport, Dnipro, 49010 Ukraine*
*e-mal: vlad.me4nik@ukr.net
**e-mail: vasylkolod56@gmail.com

Abstract—Using the method of powder metallurgy, we studied the effect of CrB₂ additives (0−8 wt %) on the formation of the structure of the diamond−matrix transition zone and the matrix material, microhardness, elastic modulus, and fixation of diamond grains in a Fe−Cu−Ni−Sn matrix and determined the wear resistance of sintered composite diamond-containing materials (DCMs). Micromechanical and tribological tests were carried out using composite samples 10 mm in diameter and 5 mm thick. The transition zone structure depends significantly on the concentration of CrB₂ in the composite and has a different nature than the structure of the matrix material. The structure of the DCM transition zone based on the 51Fe−32Cu−9Ni−8Sn matrix consists of Cu, α-Fe, and Ni₃Sn phases with graphite inclusions, and with the addition of CrB₂, it consists of the α-Fe phase and Fe₃C, Cr₇C₃, and Cr₃C₂ carbide layers without graphite inclusions. The hardness and elastic modulus of the matrix material of the sintered composites linearly increase with an increase in the concentration of CrB₂ in their composition, while the wear rate decreases. The addition of 2 wt % of CrB₂ to the 51Fe−32Cu−9Ni−8Sn composite increases hardness from 4.475 to 7.896 GPa and an elastic modulus from 86.6 to 107.5 GPa and decreases the wear rate from 21.61×10^{-6} to 10.04×10^{-6} mm³ N⁻¹ m⁻¹. The mechanism for improving the mechanical properties and decreasing the wear resistance of DCM samples containing CrB₂ additive consists in grain refining of the matrix phases of iron and copper from 5−40 to 2−10 µm and in binding carbon released during graphitization of diamond grains into nanosized carbides Fe₃C, Cr₇C₃, and Cr₃C₂. This, in turn, increases the ability of the matrix material to keep diamond grains from falling out during the operation of DCMs. The coarse-grained structure and the formation of graphite inclusions in the diamond−matrix transition zone explain poor mechanical and tribological properties of the initial (51Fe−32Cu−9Ni−8Sn) composite, causing its premature destruction and falling out of diamond grains from the DCM matrix.

Keywords: composite, diamond−matrix transition zone, composition, concentration, structure, hardness, elastic modulus, wear rate

INTRODUCTION

Composite diamond-containing materials (DCMs) are widely used in various industries, including the development of high-performance cutting wheels, wire saws, drill bits, grinding, and other tools [1−3]. DCMs based on metal matrices containing iron, copper, nickel, and tin occupy a special place among these materials [4−11]. DCMs based on Fe−Cu−Ni−Sn matrices are characterized by a wide range of physical and mechanical properties, chemical inertness to coolant reagents, low cost of starting materials, and the ductility of the matrix components to cold pressing [12−14]. The properties of such DCMs are determined by the chemical composition, structure, and morphology, which, in turn, depend on the properties of their constituents, methods and technological modes of sintering [15−17], grain sizes [18,

19], and dislocation density [20]. Under industrial conditions, DCMs are sintered by hot pressing, cold pressing followed by sintering with hot curing, vacuum sintering, etc. Such DCMs, depending on their composition and method of formation, are sintered at temperatures 700 to 1000°C and pressures 20 to 1000 MPa [21].

At the same time, these DCMs have disadvantages: insufficient hardness of the matrix material, low compressive strength, and the presence of a diamond−matrix transition zone, in which graphite inclusions appear as a result of graphitization of diamond grains during sintering [10, 13, 22]. This leads to the destruction of the transition zone by the mechanism of intense cracking and premature falling out of diamonds from the matrix and, consequently, wear of the DCM [3, 6, 22, 23]. In this regard, the material of the DCM matrix designed for tribologically intensive use should have high resistance to abrasive wear, prevent diamond grains from falling out, and have strength from fatigue and high elastic and plastic properties [24−27]. To optimize and predict the properties of DCMs, it is also necessary to take into account the fact that the elastic properties of the matrix change depending on the volumetric concentration of the components [27, 28], contact loads [29], temperatures [30−34], and the "degree" of equipping the working surface of the tool with composite materials [35]. In this regard, it is essential to study the wear resistance of existing DCMs and create new materials with the necessary complex of physical and mechanical properties.

To improve the mechanical properties of DCMs, transition metal compounds are added to their composition in a small amount compared to the main components [36, 37]. Zhang and Chen [38] considered three main strengthening factors, explaining the improvement of the mechanical properties of composites when solid particles are introduced into their volume. The addition of VN nanopowder to the 51Fe−32Cu−9Ni−8Sn initial charge with a powder size of 5−50 μm made it possible to form a structure with a grain size of 20−400 nm with dense intergrain boundaries by hot pressing at a temperature of 1000°C [39]. Using modern methods of analysis and nanoindentation, the elemental and phase composition, morphology, and mechanical (hardness, elastic modulus) and tribological (friction force, wear rate) properties of the material 49.47Fe−31.04Cu−8.73Ni−7.76Sn−3VN (a matrix for DCMs) depending on the vacuum sintering temperature were studied [40, 41]. The presence of a nanostructure in the Fe−Cu−Ni−Sn−VN matrix causes an increase in hardness and a decrease in the coefficient of friction and wear rate [42]. The mechanism for improving the properties of these composites is that VN dissolves in γ-Fe during sintering and precipitates as a fine-grained phase upon cooling.

The addition of VN nitride powder in an amount of 2%[1] to the DCM composition based on the Fe−Cu−Ni−Sn matrix ensures an increase in the ultimate strength in compression and bending and a twofold decrease in the wear rate [43]. Han et al. [44] studied the effect of the VN concentration (0−4%) on the structure, hardness, bending strength, relative density, diamond fixation in the matrix, and the friction coefficient of a DCM based on a Fe−Cu matrix sintered by powder metallurgy. In particular, the addition of 2% of VN to the Fe−Cu-based DCM led to an increase in its bending strength and hardness by 25 and 20%, respectively; the wear resistance decreased from 3.99 to 2.06 μm due to narrowing the gap between the diamond grain and the matrix [44]. A further increase in the VN concentration in the composite leads to a deterioration in its mechanical properties. However, the processes of the formation of nanoscale heterogeneities in the diamond−matrix transition zone and their effect on the mechanical and tribological properties of DCM remain unexplored.

The addition of 2% of CrB_2 micropowder to the 51Fe−32Cu−9Ni−8Sn matrix ensures decarburization in the diamond−matrix transition zone through the formation of nanostructured layers of Cr_3C_2, Cr_7C_3, Fe_3C, and $Cr_{1.65}Fe_{0.35}B_{0.96}$ and increases the wear resistance of DCM [45, 46]. In [47], the effect of the CrB_2 concentration (0−8%) on the structure, microhardness, elastic modulus, friction coefficient, and wear resistance of the Fe−Cu−Ni−Sn composite matrix formed by cold pressing followed by sintering with hot curing is investigated. An increase in the CrB_2 concentration in the composite is accompanied by an increase in its hardness and elastic modulus. The coefficient of friction and the wear rate decrease with the concentration of CrB_2 increasing to 2%; with a further increase, the wear rate grows. A significant increase in the wear resistance of the sample containing 2% of CrB_2 in comparison with the initial sample is due to the formation of a fine-grained structure and an optimal combination of hardness and elastic modulus. There are no data in the literature on the effect of the CrB_2 concentration on the formation of the structure of the diamond−matrix transition zone of the DCM, which can affect the fixation of diamond grains in the Fe−Cu−Ni−Sn matrix or the properties and wear resistance of composite materials sintered by powder metallurgy process. Studies of the relationship between the structure of the diamond−

---

[1] Hereinafter, the composition of the DCM is given in wt %.

Table 1. Composition of the initial mixtures for sintering the samples of DCM matrix material, wt %

Sample	Fe	Cu	Ni	Sn	CrB$_2$
1	51	32	9	8	–
2	49.98	31.36	8.82	7.84	2
3	48.96	30.72	8.64	7.68	4
4	47.94	30.08	8.46	7.52	6
5	46.92	29.44	8.28	7.36	8

matrix transition zone and the mechanical properties and wear resistance of the material of the DCM matrix, considered now, have not been carried out either. Due to the lack of the necessary knowledge in this field, we cannot affect the structure formation and form purposefully, by one method or another, a DCM with high performance characteristics.

The goal of this work was to study the effect of adding CrB$_2$ powder (0−8%) on the formation of the structure of the Fe−Cu−Ni−Sn matrix, its physical and mechanical properties, the fixation of diamond grains in the matrix, and the wear resistance of composite diamond-containing materials formed by cold pressing followed by hot curing.

EXPERIMENTAL

Starting Materials and Method of Sintering

We used powders of iron PZh1M2, copper PMS-1, nickel PNE, tin PO-1 (Zavod poroshkovoi metal-lurgii, Ukraine), and chromium diboride CrB$_2$ (70.62% of Cr and 29.30% of B). Initial mixtures for sintering the samples of the DCM matrix and materials, with a diameter of 10 mm and a thickness of 5 mm, were prepared by pressing at room temperature with subsequent sintering in a SNOL 72/100 furnace with hot curing at a pressure of 200 MPa. The output powders had a dispersity of 5−50 μm. The compositions of the initial mixtures for sintering the samples of the DCM matrix material are given in Table 1.

The powder mixtures were dry blended in an off-axis mixer for 8 h. The specific power of the mixer was 8 W/h. The prepared mixtures were pressed at room temperature in a hydraulic press in molds made of the heat-resistant alloy KhN77TYuR (*GOST 5632-72*) at a pressure of 500 MPa. The compacts were sintered in the same molds in a SNOL 72/100 furnace at 800°C for 1 h, followed by hot curing at a pressure of 200 MPa. Diamond-containing mixtures for sintering DCM samples were obtained as follows: diamond powder of AC160T grade, 400/315 grain size, moistened with glycerin, was added to the prepared powder mixtures (Table 1) in an amount of 1.54 carats per 1 cm^3 of the charge (which corresponds to the relative concentration $K = 35\%$) and evenly mixed in an alcoholic medium. To prevent a sharp drop in temperature during hot curing of the composite, the press surfaces in contact were insulated with asbestos material. The temperature of the system during hot curing decreased from 800 to 750°C (cooling rate ~10°C/min). After sintering, the blanks of the matrix and DCM samples were ground to obtain cylinders 9.62 mm in diameter and 4.84 mm in thickness. Before microstructural, mechanical, and tribological studies, the surface of the sintered samples was polished with a diamond paste with 1-μm particles and a colloidal solution with particles of silicon oxide with a size of 0.04 μm until a mirror surface was obtained.

Microstructure and Micromechanical Characteristics of Samples

The morphology of the initial powders and the microstructure of the sintered DCMs were investigated by scanning electron microscopy (SEM) using a REM-106I scanning electron microscope (SELMI, Ukraine) with an acceleration potential of 30 kV. The chemical compositions were calculated using the ZAF correction method and the Magallanes 3.1 software package. Electron microscopic studies of thin foils obtained from the sintered samples were carried out using a TEM-125 transmission electron microscope (Sumy, Ukraine) with an acceleration potential of 125 kV at a resolution of 0.18 nm. X-ray diffraction patterns of the samples were obtained using a DRON 4.1C diffractometer in the radiation of a copper anode in the Bragg−Brentano geometry in the angle range of $20° \leq 2\theta \leq 80°$. X-ray phase analysis was carried out by the conventional procedure using the X-powder software package [48]. The diffraction spectrum of the samples in the form of a set of refined values of the interplanar spacing d_i of the crystal lattice of the composite phase and the relative intensity of reflections of this phase I_i was identified by comparison with the reference sample, using the ASTM-ICPDS card index [49].

The microindentation tests were performed using polished sintered samples. The measurement was carried out using a Micro Gamma universal complex for micromechanical testing [50, 51] in the mode of continuous indentation of a Berkovich indenter. The load diagrams $P–h$ were obtained by recording the indentation force P and the indentation depth h during the test [52]. The maximum indenter load was 0.5 N, and the loading speed was 50 mN/s. Twelve measurements were carried out for each sample with a step of 50 μm between indentations. The microhardness H and the elastic modulus E were found by analyzing the indenter unloading curve by the method of Oliver and Pharr [53]. The measurement results were corrected according to the procedure presented in [54].

Tribological Testing of Samples

Tribological tests of the sintered samples were carried out at an ambient temperature of 25°C and relative humidity of 50% using a Micro Gamma device, the schematic diagram of which is presented in [51]. We used a pin-on-disk testing mode with reciprocating friction [55] and the ball—ground section mode (calo-test) using a friction machine [40]. The surfaces of the samples were prepolished using SiC materials with a particle size up to 5 μm and an oxide suspension based on colloidal particles of silicon dioxide with a particle size of 100 nm.

The reciprocating-friction tests of the sintered samples were carried out using a diamond conical indenter with a radius of curvature at the apex of 50 μm at a load of 500 mN and a sliding speed of 20 μm/s. The number of cycles was 300. The wear of friction tracks was measured using contactless interference 3D Mico Alpha profilometers [56, 57], which records surface irregularities with nanometric precision [58]. This enables the measurement of volume V of the friction track. Based on the experimental data obtained, the wear rate was determined by the equation [59]

$$I = \frac{V}{P_{\mathrm{N}} L n},$$

where V is the volume of the friction track (loss of volume, wear a sample), μm³; P_{N} is the applied normal force, N; L is the track length (distance traveled by the indenter in one cycle), μm; and n is the number of cycles. Tests comply with international standards *ASTM G99-959*, *DIN50324*, and *ISO 20808* [60, 61].

The tests of the sintered samples in the ball—ground section test with abrasive wear of the sample by a ball made of 100Cr6 steel with a radius of 10 mm were carried out at a load of 1 N with the addition of a suspension containing 20% of diamond powder with a dispersion of 0.5—1.0 μm. The speed of rotation of the ball was 72 rpm, and the duration of the process was 1500 s. The abrasive wear resistance and the volume V of the wear hole were determined by the diameter of the indentation D of the balls when rubbing against the sample's surface. Volume V of the wear hole was calculated from the condition of equality of the radius of hole curvature with the radius of the ball R by the equation $V = \pi D^4/(64R)$. The wear of the friction track was measured using a Micro Alpha contactless interference 3D profilometer [56].

The Micro Gamma tester was used in [41, 42, 62] to study the kinetics of wear of composite materials based on multicomponent metal matrices and ceramic materials under reciprocating friction.

RESULTS AND DISCUSSION

Morphology of Starting Materials

SEM images of the initial mixture of iron, copper, nickel, and tin powders are presented in Fig. 1a. A relatively uniform distribution characterizes the components in the mixture; their size varies in the range of 5—25 μm. Iron powder particles, represented by larger dark gray particles against the background of lighter small particles with an average size of 10—25 μm, have an irregular (stone-like) shape. Larger iron particles are also observed, which are formed by the adhesion of smaller agglomerate particles.

Particles of copper powder 5—15 μm in size have a less dense and thinner spatial dendritic structure with pronounced branches, which leads to a decrease in the relative bulk density and prevents their dense packing in a bulk state. Nickel powder particles with an average size of 5—10 μm have a rounded shape with a very dense structure, which, as in iron powders, causes a high packing density in the bulk state. Tin powder particles are spherical, although elongated particles are also observed. Beads of metal and small particles (satellites) are seen on their surface. The round shape of the particles is suitable for their dense packing in a bulk state.

Particles of CrB_2 powder in the 49.98Fe—31.36Cu—8.82Ni—7.84Sn—2CrB$_2$ initial mixture are evenly distributed on particles of iron, copper, nickel, and tin and do not form a solid framework or bulk agglom-
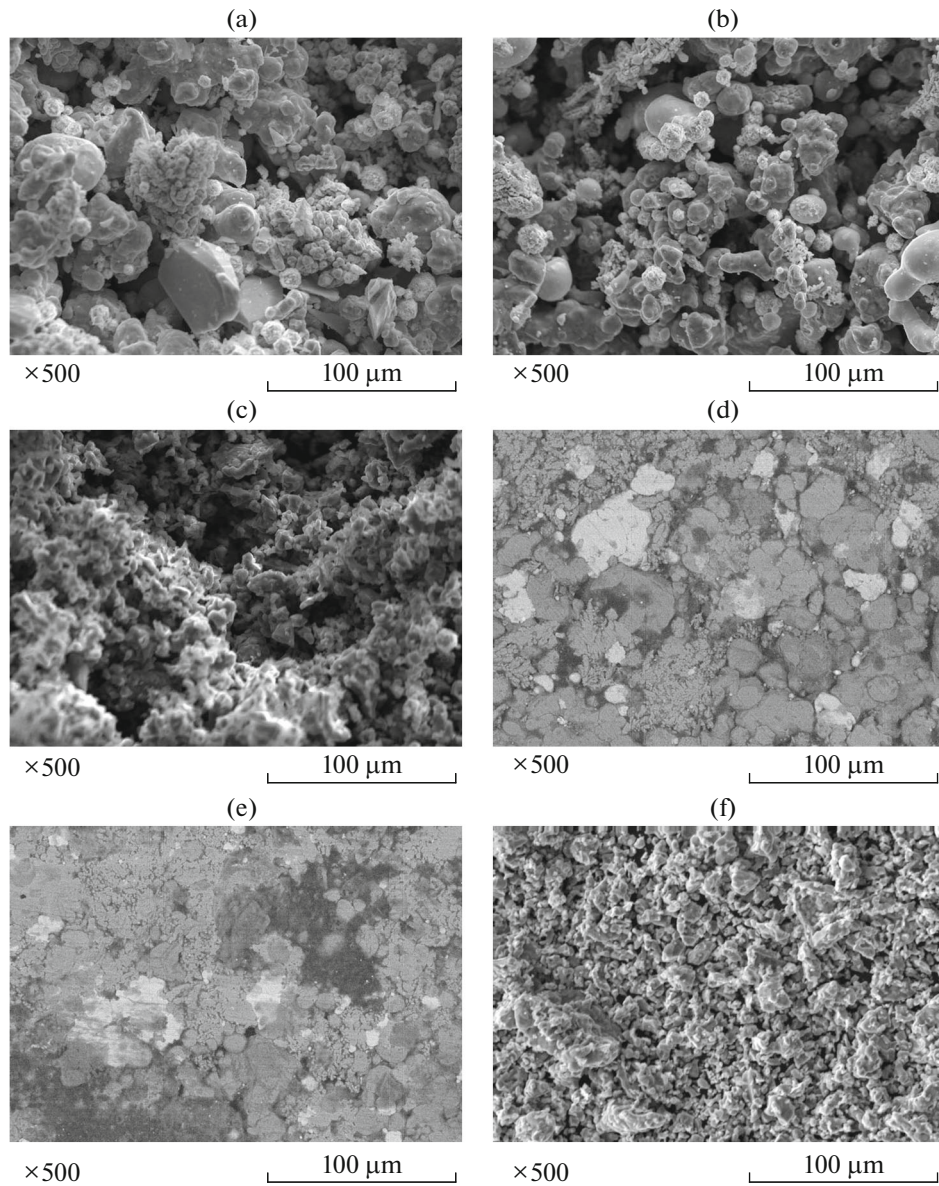
Fig. 1. SEM images of mixtures (a) 51Fe−32Cu−9Ni−8Sn and (b) 49.98Fe−31.36Cu−8.82Ni−7.84Sn−2CrB$_2$ and (c) a CrB$_2$ powder in the initial state and (d−f) as corresponding briquettes cold-pressed at 500 MPa, respectively.

erate (Fig. 1b). The morphology of the initial CrB$_2$ powder introduced into a mixture of iron, copper, nickel, and tin powders is shown in Fig. 1c. The grain size of the CrB$_2$ powder is in the range from 0.5 to 7 μm. Large particles of CrB$_2$ powder are observed, formed, most likely, by the adhesion of smaller particles. According to [46], CrB$_2$ particles have a single-phase structure with lattice parameters $a = 0.2972$ nm and $c = 0.3069$ nm.

During the pressing of the 51Fe−32Cu−9Ni−8Sn mixture, all of its components are deformed by contact with each other (Fig. 1d). The shape and size of iron particles (large grains of light and gray color) and nickel (smaller particles of gray color) do not change, while the particles of copper and tin have changed in both shape and size. The mixture components are compacted by adjusting the surfaces of adjacent particles to each other. Such a powder pressing mechanism promotes an increase in the contact area, which is crucial for the sintering of these systems. The structure of a briquette obtained from a mixture of 49.98Fe−31.36Cu−8.82Ni−7.84Sn−2CrB$_2$ is characterized by a uniform distribution of CrB$_2$ grains (fine grains of light color) throughout the volume of the material (Fig. 1e). CrB$_2$ particles are in close contact
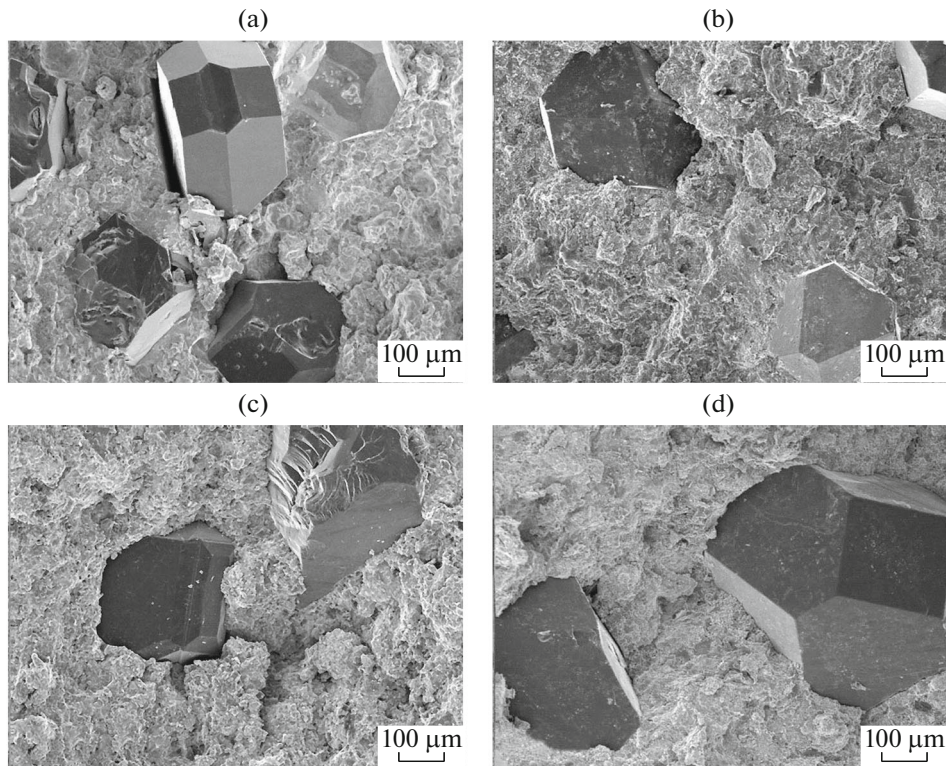
Fig. 2. Micrographs of the fracture surface of sintered DCM samples (a) without additives and with the addition of (b) 2, (c) 4, and (d) 6% of CrB$_2$.

with the components of the charge, which can improve mutual solubility and affect the formation of new phases and, consequently, the physical and mechanical properties of the material. There are no signs of welding in the fractograms of CrB$_2$ powder pressing (Fig. 1f). The shape of the CrB$_2$ powder particles remained practically unchanged.

Microstructure and Features of the Diamond−Matrix Contact of Sintered Samples

SEM images of sections of sintered DCM samples (Fig. 2) illustrate the features of the diamond−matrix contact.

In the DCM samples, diamond grains are located nonuniformly; their sizes are in the range of 300−450 μm. In sample 1, there are gaps and discontinuities at the diamond−matrix interface, and pits are also observed that were formed as a result of diamond grains falling out of the DCM matrix (see Fig. 2a). In samples 2−4 containing CrB$_2$ additives, the diamond−matrix contact was dense, without visible gaps or discontinuities (Figs. 2b−2d). On the surface of their fracture, no pits from the precipitated diamond grains are found. The mechanism of adhesion of diamond grains to the metal DCM matrix has not yet been sufficiently studied. The adhesion of the diamond−matrix contact is explained by molecular, electrostatic, and chemical interactions, changes in energy and structural states, and metal clamping. Most often, the adhesion strength is due to the simultaneous action of several of these factors. The effect of each factor changes depending on the nature of the materials, their physicomechanical and chemical properties, and production conditions.

The structures of the studied samples differ. The grains of the 51Fe−32Cu−9Ni−8Sn DCM matrix (sample 1) are 5−40 μm; there are thin, well-formed boundaries between the grains, and pores are present in the boundaries. At the same time, discontinuities and gaps are observed at the diamond−matrix interface (Fig. 3a).

Regarding the X-ray microanalysis data, we can assume that the structure of this sample consists of a BCC solid solution based on α-Fe, contains a small amount of nickel, copper, and tin (An1, Table 2), an FCC solid solution based on Cu (An2, Table 2), and a solid solution of nickel and iron in a double compound of the Cu−Sn system (γ-phase, An3, Table 2).
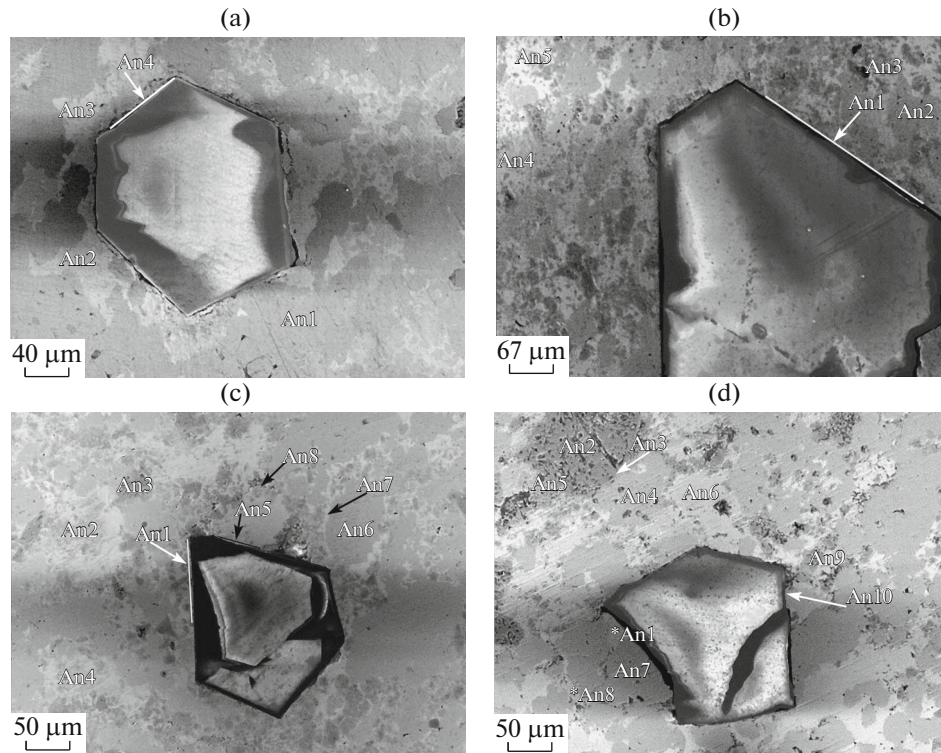
Fig. 3. SEM images of the surface of sintered DCM samples with different concentration of CrB$_2$: (a) 0, (b) 2, (c) 4, and (d) 6%.

The introduction of 2% of CrB$_2$ powder into the 51Fe−32Cu−9Ni−8Sn composite (sample 2) leads to structure refinement; that is, the sizes of the main components, in particular, iron and copper, decreased from 5−40 to 2−10 μm (Fig. 3b). The diamond−matrix contact becomes dense and does not contain visible gaps and pores. The structure of this DCM is formed with a BCC solid solution based on α-Fe (An4, An7, Table 2), an FCC solid solution with different concentrations of elements (with a predominance of copper) (An1, An6, An8, An10) or iron (An5), and a solid solution based on CrB$_2$ (An2). In samples 3 and 4, containing 4 and 6% of CrB$_2$, respectively, β- and γ-phases in the double compound of the Cu−S, that is, An5 and An7 systems, respectively were found (Table 2), but the size of the main phases in them is larger than in sample 2 and reaches 15 μm (Figs. 3c and 3d). The phase composition of sample 5, containing 8% of CrB$_2$, is similar to sample 4 and differs only in the concentration of components in solid solutions.

These results are in good agreement with the results of [46]. For example, according to [46], the structure of sample 1 consists of phases α-Fe (crystal lattice parameter $a = 0.28680$ nm), Cu ($a = 0.36087$ nm), Cu$_9$NiSn$_3$ ($a = 1.8020$ nm), and NiSn$_3$ ($a = 0.5296$ nm, $c = 0.4283$ nm) with a grain size of 5−20 μm. The crystal structure of the components and the phase composition of the composite were determined: Cu 47.2−4.6%, Fe 30.6−3.8%, Cu$_9$NiSn$_3$ 15.1−2.1%, and Ni$_3$Sn 7.1−2.5%. The introduction of 2% of CrB$_2$ powder into the 51Fe−32Cu−9Ni−8Sn composite leads to structure refinement; that is, the sizes of the main components, particularly iron and copper, decreased from 5−20 to 2−4 μm. The structure of this composite consists of phases α-Fe ($a = 0.2877$ nm), Cu ($a = 0.3689$ nm), Cu$_9$NiSn$_3$ ($a = 1.801$ nm), NiSn$_3$ ($a = 0.52958$ nm, $c = 0.4281$ nm), and CrB$_2$ ($a = 0.2972$ nm, $c = 0.3069$ nm). Isolated CrB$_2$ inclusions are located both along the grain boundaries and in bulk and practically disappear at the interphase boundaries.

Thus, the addition of 2 to 6% of CrB$_2$ powder to the 51Fe−32Cu−9Ni−8Sn composite (samples 2−4) refines the structure and contributes to the formation of a tight contact at the diamond−matrix interface, without pores or gaps (Figs. 3b−3d). Similar patterns were studied for the DCM based on the Fe−Cu matrix [44]. According to [44], the addition of 2% of VN to the composition of a Fe−Cu-based DCM resulted in an increase in bending strength by 25% and hardness by 20%. The wear resistance decreased from 3.99 up to 2.06 μm due to the structure refinement and a narrowing the gap between the diamond

Table 2. X-ray spectrometry analysis of the sintered DCM samples with different CrB_2 concentrations

Sample	Notation	Concentration of elements, wt %					Phases
		Fe	Ni	Cu	Sn	Cr	
1	An1	99.3	0.3	0.4	—	—	α_{Fe}
	An2	3.3	1.0	85.4	12.3	—	γ_{Cu}
	An3	1.2	9.2	54.1	35.5	—	γ_{Cu-Sn}
	An4*	40.4	9.3	30.0	20.3	—	
2	An1	16.4	5.7	74.0	1.8	2.1	γ_{Cu}
	An2	3.9	0.8	2.7	0.8	91.8	CrB_2
	An3*	5.2	19.0	44.2	8.1	23.5	
	An4	98.0	1.0	1.0	—	—	α_{Fe}
	An5	45.8	4.6	39.2	6.2	4.2	α_{Fe}
	An6	—	1.5	96.3	2.2	—	γ_{Cu}
	An7	95.3	1.5	2.6	—	0.6	α_{Fe}
	An8	10.4	8.5	71.4	7.9	1.8	γ_{Cu}
	An9	18.8	8.5	37.5	15.0	20.2	γ_{Cu}
	An10	6.9	4.2	69.2	12.8	7.1	γ_{Cu}
3	An1	2.4	10.6	69.3	11.0	6.7	γ_{Cu}
	An2	96.8	1.7	0.9	—	0.6	α_{Fe}
	An3*	1.3	16.5	34.7	5.8	41.7	
	An4*	12.3	12.7	39.6	13.3	22.1	
	An5*	21.5	10.7	30.0	21.8	16.0	
	An6	1.9	—	1.3	—	96.8	CrB_2
	An7	0.7	14.7	45.6	37.9	1.1	γ_{Cu-Sn}
	An8	0.6	58.6	17.1	13.8	9.9	γ_{Ni}
4	An1*	2.2	24.9	24.0	6.9	42.0	
	An2	—	4.2	85.4	6.4	4.0	γ_{Cu}
	An3	2.7	5.6	5.5	1.0	85.2	CrB_2
	An4	4.1	5.4	73.2	11.8	5.5	γ_{Cu}
	An5*	39.8	7.1	41.2	8.9	3.0	
	An6	99.3	0.7	—	—	—	α_{Fe}
	An7	5.6	16.5	39.7	38.2	—	γ_{Cu-Sn}
	An8*	1.2	15.2	39.4	7.7	36.5	
	An9	—	3.1	82.0	12.8	2.1	γ_{Cu}
	An10	1.5	—	2.6	—	95.9	CrB_2

* The result can be ambiguous; scanning was possibly carried out in the area containing the mixture of phases.

grain and the matrix. The authors of [44] also indicated that a further increase in the VN concentration in the DCM composition leads to a deterioration in its mechanical properties. However, the nature of the adhesion of diamond grains to the DCM metal matrix has not been established. The processes of the formation of nanoscale heterogeneities in the diamond−matrix transition zone and their effect on the mechanical and tribological properties of DCM remain unexplored.

Micrograph images of the diamond−matrix interface, obtained by transmission electron microscopy (TEM), for sintered samples 1 and 2 are presented in Fig. 4. The structure of the transition zone of samples 1 (Figs. 4a and 4b) and 2 (Fig. 4c and 4d) significantly differs from the structure of the matrix material
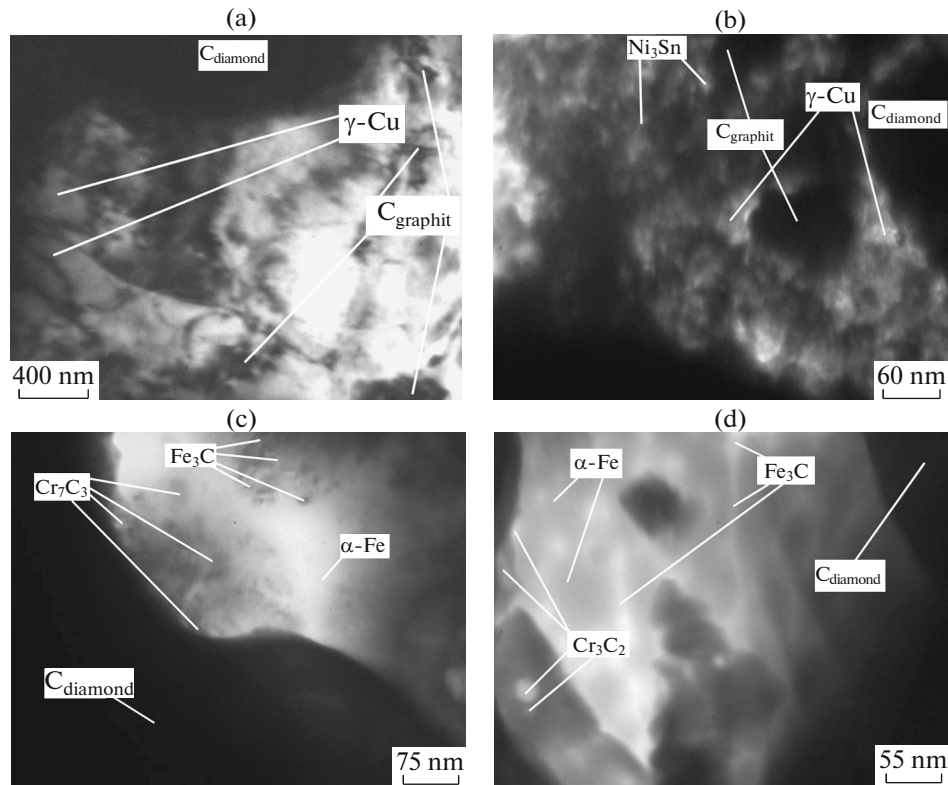
Fig. 4. TEM images of the microstructure regions of the diamond−matrix transition zone of the DCM samples (a, b) 1 and (c, d) 2.

(Fig. 3, Table 1). The structure of the transition zone of sample 1 consists of phases Cu and Ni_3Sn with graphite inclusions (Figs. 4a and 4b), which is the reason for its premature destruction and the falling out of diamond grains from the matrix material (Figs. 2a, 3a, 5a, and 5b). At the same time, the structure of the transition zone of sample 2, containing 2% of CrB_2, consists of α-Fe phases and nanoscale layers with Fe_3C, Cr_7C_3, and Cr_3C_2 without graphite inclusions (Figs. 4c and 4d), which increases the ability of the matrix to hold diamond grains against falling out during operation. This is because the carbon, released as a result of graphitization along the surface layers of diamonds, becomes bonded into carbides, which improves the ability of the matrix of samples 2−4 to retain diamonds from falling out (Figs. 7b−7d and 8b−8d).

These effects are most pronounced at the optimal concentration of CrB_2 in the composite. Incorrect and/or improper selection of the CrB_2 concentration in the initial charge deteriorates the service properties of the DCM. In particular, in the matrix of sample 5, containing 8% of CrB_2, cracks are observed near the diamond grain along the entire height of the diamond-containing layer (Fig. 5c). The data obtained allow us to assume that for sample 2, in contrast to samples 1 and 3−5, an increased wear resistance should be expected.

Mechanical and Tribological Properties of Samples

The results of studying the physical and mechanical properties (hardness and elastic modulus) of the 51Fe−32Cu−9Ni−8Sn DCM matrix material with different CrB_2 concentrations are shown in Fig. 6. Analysis of these dependences showed that for sample 1 ($CrB_2 = 0\%$) (Fig. 6a), hardness and elastic modulus values are 4.475 and 86.6 GPa, respectively. In sample 2, with an increase in the CrB_2 concentration to 2%, the hardness and elastic modulus increase values increase to 7.896 and 107.5 GPa, respectively. With an increase in the CrB_2 concentration from 2 to 4% (sample 3) and from 4 to 6% (sample 4), hardness increases less intensively than in sample 2 containing 2% of CrB_2. With a further increase in the CrB_2 concentration from 6 to 8% (sample 5), the hardness increases from 8.586 to 10.201 GPa, and the modulus of elasticity increases from 115.6 to 168.6 GPa. Two reasons can cause sach a change in the mechanical
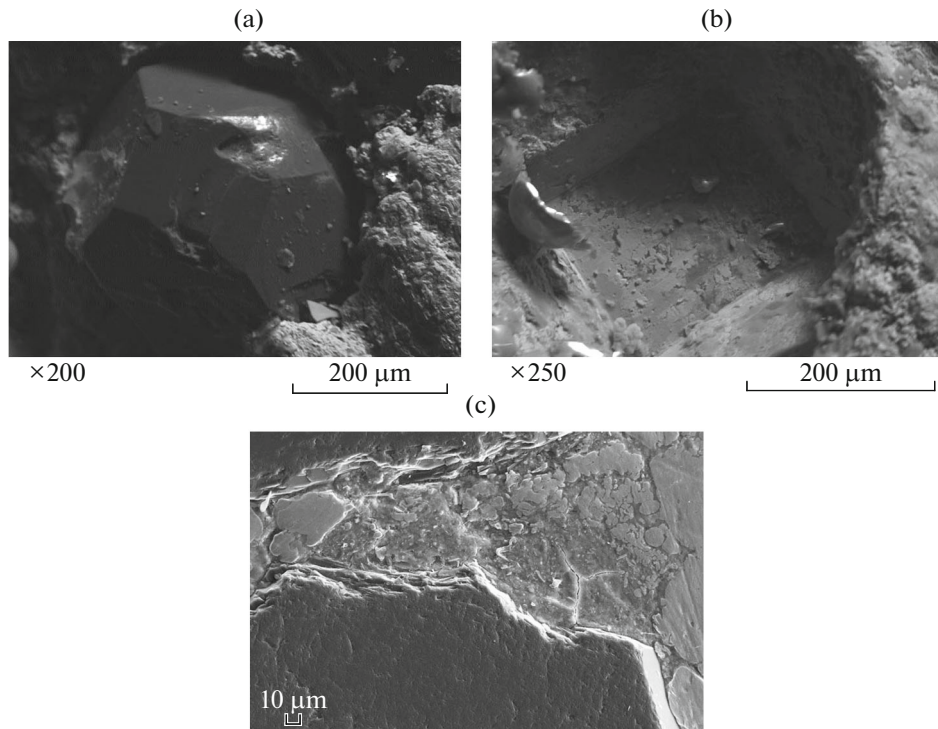
(a) (b)

×200   200 μm   ×250   200 μm

(c)

10 μm

Fig. 5. SEM images of the working surface of (a, b) the DCM sample 1 after its operation and (c) sample 5.

properties with increasing CrB_2 concentration; each of these reasons could lead to such a result separately, or the effect is the result of their joint action. One reason is the direct action of the CrB_2 addition on the properties of the composite. The mechanical properties of CrB_2 (microhardness, elastic modulus, ultimate compressive strength) are significantly higher than those of the main components of the composite (iron, copper, nickel, and tin). Another reason is the difference in the structure of composites containing CrB_2 additives [46]. The results of determining the hardness of the sintered samples are consistent with the hardness data for DCM samples, based on the Fe−Cu−Ni−Sn matrix with additions of CrB_2 and obtained by hot pressing [12].

The change in the topography of the friction tracks (width and depth of the wear groove) during the reciprocating friction of the matrix material of sintered samples 1 and 2, depending on the CrB_2 concentration, is illustrated in Fig. 7. The width and depth of the wear groove for DCM sample 1 (Fig. 7a) is much larger than those for DCM sample 2 (Fig. 7b). With a further increase in CrB_2 concentration (C_{CrB_2}), the depth and width of the wear groove change in a different way. The wear rate I of the matrix material of the sintered samples, depending on the concentration of CrB_2 (C_{CrB_2}), are given in Table 3. The values of these parameters differ depending on the concentration of CrB_2 (C_{CrB_2}) in the initial mixture. In sample 1 ($C_{CrB_2} = 0\%$) (Table 3), the wear rate is 21.61×10^{-6} mm³ N⁻¹ m⁻¹. In sample 2, with an increase in C_{CrB_2} from 0 to 2%, the wear rate decreases from 21.61×10^{-6} to 10.04×10^{-6} mm³ N⁻¹ m⁻¹.

The increased wear resistance of sample 2 compared to sample 1 can be explained by finer grain (Figs. 3a and 3b) and higher hardness and elastic modulus. With an increase from 2 to 4% (sample 3), the wear rate I begins to increase gradually. With a further increase in the composition of the initial charge (samples 4 and 5), the wear rate continues to increase gradually.

The maximum wear rate of 21.61×10^{-6} mm³ N⁻¹ m⁻¹ was recorded for sample 1, which does not contain CrB_2, which correlates with hardness and elastic modulus.

The tribological tests of the sintered samples in the ball−ground section test mode with abrasive wear also showed a significant change in properties due to the physical nature and structure. Typical images of the wear areas of sintered samples 1 and 2 after friction with a steel ball 10 mm in diameter at a load of 1 N and a rotation speed of 72 rpm for 1500 s are shown in Fig. 8; it is seen that the sizes of the wear holes of these samples also differ. The largest diameter of the wear hole is observed for sample 1 (Fig. 8a), and the
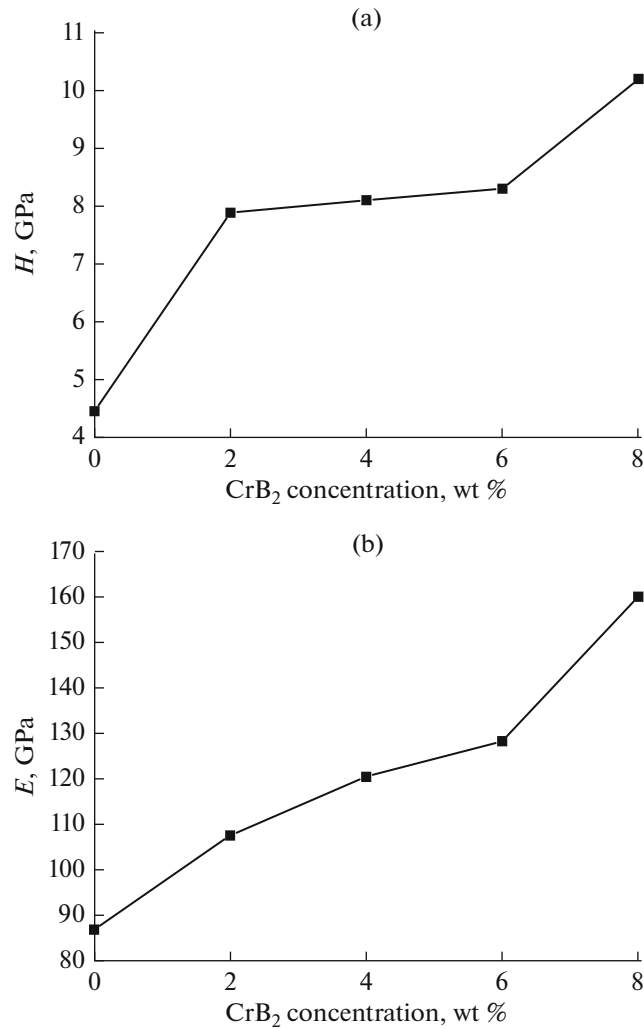
Fig. 6. Dependences of (a) hardness H and (b) elastic modulus E on the CrB$_2$ concentration in the 51Fe−32Cu−9Ni−8Sn composite.

smallest, for sample 2 (Fig. 8b). With a further increase in the concentration of CrB$_2$ (C_{CrB_2}), the diameter of the wear hole for samples 3−5 increases slightly compared to sample 2. The wear rate I of the matrix material of the sintered samples depending on the concentration of CrB$_2$ (C_{CrB_2}) are given in Table 4; an increase in concentration also decreases the wear rate I. The introduction of 2% of CrB$_2$ in the initial 51Fe−32Cu−9Ni−8Sn charge decreases the wear rate from 3.38×10^{-3} to 1.59×10^{-3} mm^3 N^{-1} m^{-1}. The increased wear resistance of sample 2 in comparison with sample 1 can be explained, as mentioned above, by finer grain (Figs. 3a and 3b) and higher values of hardness and elastic modulus. With an increase in the

Table 3. Tribological characteristics of the matrix material of the sintered samples

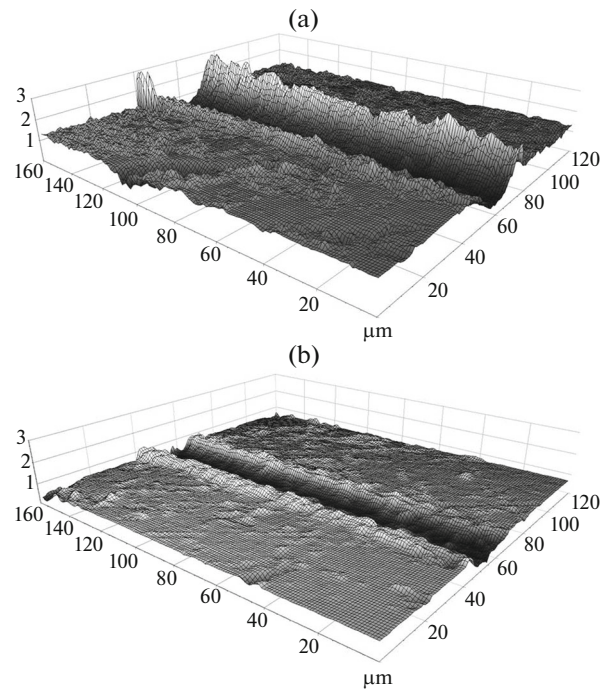| Sample	Concentration C_{CrB_2}, %	V, 10^{-6} mm^3	I, 10^{-6} mm^3 N^{-1} m^{-1}
1	0	5.84	21.61
2	2	2.08	10.04
3	4	3.22	12.10
4	6	3.54	13.26
5	8	4.20	15.66

(a)

(b)

Fig. 7. 3D images of the sections of the friction tracks of the matrix material of the sintered samples (a) 1 and (b) 2.

concentration of CrB_2 to 4% in the initial $51Fe-32Cu-9Ni-8Sn$ charge (sample 3), the wear rate gradually increases to 1.59×10^{-3} mm^3 N^{-1} m^{-1}. With a further increase of CrB_2 in the composition of the initial charge (samples 4 and 5), the wear rate continues to gradually increase to 2.12×10^{-3} and 2.65×10^{-3} mm^3 N^{-1} m^{-1}, respectively. The increase in wear resistance, taking into account the addition of CrB_2 to the composite, is due to the same reasons as in the case of reciprocating friction discussed above.

Thus, the studies showed CrB_2 additive, depending on its concentration in the $51Fe-32Cu-9Ni-8Sn$ composite, ensures a twofold decrease in the wear rate. The mechanism for increasing the mechanical properties (hardness and modulus of elasticity) and wear resistance of DCM samples containing CrB_2 is that carbon, which is released during graphitization of the surface layers of diamond grains, is bonded into carbides Fe_3C, Cr_7C_3, and Cr_3C_2 (Figs. 4c and 4d). This improves the ability of the matrix material to retain diamond grains from falling out during the DCM operation (Figs. 2b−2d and 3b−3d). The structure of the transition zone of sample 1 consists of phases Cu and Ni_3Sn with graphite inclusions (Figs. 4a and 4b), which is the reason for its premature destruction and the falling out of diamond grains from the matrix material (Figs. 2a, 3a, 5a, and 5b). At the same time, the structure of the transition zone of the DCM sample without CrB_2 (sample 1) consists of phases Cu and Ni_3Sn with graphite inclusions (Figs. 4a

Table 4. Tribological characteristics of the matrix material of the sintered samples, determined in the ball-ground section testing mode

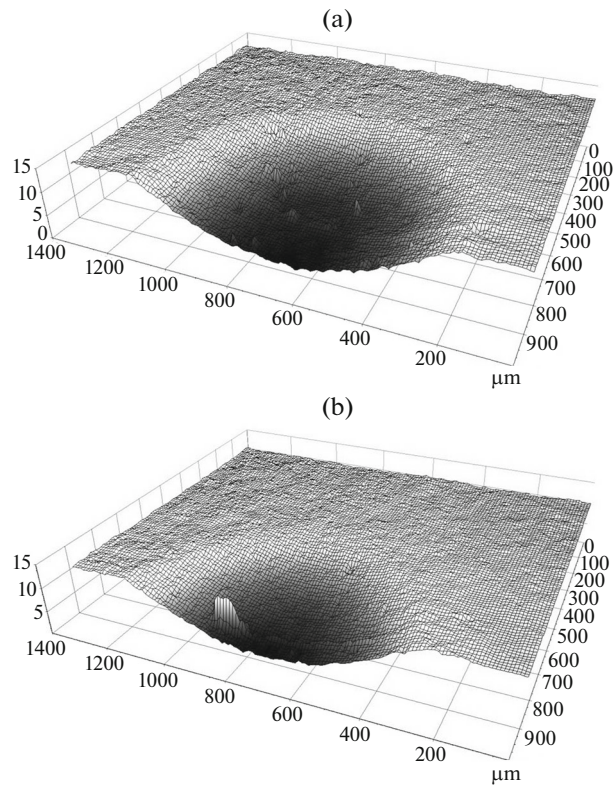| Sample	C_{CrB_2}, %	Wear hole volume V, mm^3	Wear rate I, 10^{-3} mm^3 N^{-1} m^1
1	0	0.38	3.38
2	2	0.18	1.59
3	4	0.20	1.77
4	6	0.24	2.12
5	8	0.30	2.65

Fig. 8. 3D topography of wear holes, obtained by the ball-ground section method, after rubbing with a steel ball on the surface of samples (a) 1 and (b) 2.

and 4b), which is the reason for its premature destruction and the falling out of diamond grains from the matrix material (Figs. 2a, 3a, 5a, and 5b).

CONCLUSIONS

The findings of the study of the effect of adding CrB$_2$ (0–8%) on the formation of the structure of the diamond–matrix transition zone and the matrix material, physical and mechanical properties, the fixation of diamond grains in the Fe–Cu–Ni–Sn matrix material, and the wear resistance of composite diamond-containing materials sintered by powder metallurgy are as follows.

The diamond–matrix transition zone structure substantially depends on the CrB$_2$ concentration in the composition of the initial 51Fe–32Cu–9Ni–8Sn DCM charge and has a different nature than the structure of the matrix material. The structure of the DCM transition zone based on the 51Fe–32Cu–9Ni–8Sn matrix consists of Cu, α-Fe, and Ni$_3$Sn phases with graphite inclusions. At the same time, the structure of the DCM transition zone based on the 51Fe–32Cu–9Ni–8Sn matrix with CrB$_2$ additives consists of a α-Fe matrix phase and a nanostructure with Fe$_3$C, Cr$_7$C$_3$, and Cr$_3$C$_2$ without graphite inclusions.

The hardness and elastic modulus of the composite matrix material increase linearly with an increase in the concentration of CrB$_2$ in its composition, and the wear rate decreases. A composite that does not contain CrB$_2$ additive demonstrates the lowest value of hardness (4.475 GPa), modulus of elasticity (86.6 GPa), and the highest value of the wear rate (21.61 × 10^{-6} mm^3 N^{-1} m^{-1}). The poor mechanical and tribological properties of this composite are explained by the coarse-grained structure of the matrix and the formation of graphite inclusions in the diamond–matrix transition zone, which causes its premature destruction and the falling out of diamond grains from the matrix during the operation of the DCM.

The addition of 2% of CrB$_2$ to the 51Fe–32Cu–9Ni–8Sn composite increases hardness to 7.896 GPa and an elastic modulus to 107.5 GPa and decreases the wear rate from 21.61× 10^{-6} to 10.04 × 10^{-6} mm^3 N^{-1} m^{-1}. The mechanism for improving the mechanical properties and wear resistance of the DCM samples containing CrB$_2$ consists in the fact that carbon, which is released during the graphitization of dia-

mond grains, is bound into the layers of carbides Fe_3C, Cr_7C_3, and Cr_3C_2. Other reasons are refining the grains of iron and copper from $5-40$ to $2-10$ μm and the presence of discrete zones of higher hardness with high values of the modulus of elasticity.

This, in turn, improves the ability of the matrix material to keep diamond grains from falling out during the DCM operation. Another factor contributing to the mechanical properties and decreasing the wear resistance of DCM with CrB_2 is the refinement of iron and copper grains from $5-40$ to $2-10$ μm. Tribological tests of the sintered composites in the pin-on-disk testing mode under reciprocating friction and the ball−ground section under abrasive friction, in addition to measuring the microhardness and elastic modulus, indicate the expansion of the functionality of the developed composite containing 2% of CrB_2.

FUNDING

CONFLICT OF INTEREST

The authors declare that they have no conflicts of interest.

REFERENCES

1. Bondarenko, N.A., Zhukovskii, A.N., and Mechnik, V.A., Analysis of the basic theories of sintering of materials. 1. Sintering under isothermal and nonisothermal conditions (a review), *Sverkhtverd. Mater.*, 2006, vol. 28, no. 6, pp. 3−17.

2. Borowiecka-Jamrozek, J. and Konstanty, J., Microstructure and mechanical properties a new iron-base material used for the fabrication of sintered diamond tools, *Adv. Mater. Res.*, 2014, vol. 1052, pp. 520−523.

3. Kolodnits'kyi, V.M. and Bagirov, O.E., On the structure formation of diamond containing composites used in drilling and stone working tools (a review), *J. Superhard Mater.*, 2017, vol. 39, no. 1, pp. 1−17.

4. Dai, Q.L., Luo, C.B., Xu, X.P., and Wang, Y.C., Effects of rare earth and sintering temperature on the transverse rupture strength of Fe-based diamond composites, *J. Mater. Process. Technol.*, 2002, vol. 129, pp. 427−430.

5. Zaitsev, A.A., Sidorenko, D.A., Levashov, E.A., Kurbatkina, V.V., Rupasov, S.I., Andreev, V.A., and Sevast'yanov, P.V., Development and application of the Cu−Ni−Fe−Sn based dispersion hardened bond for cutting tools of superhard materials, *J. Superhard Mater.*, 2012, vol. 34, no. 4, pp. 270−280.

6. Mechnyk, V.A., Diamond−Fe−Cu−Ni−Sn composite materials with predictable stable characteristics, *Mater. Sci.*, 2013, vol. 48, no. 5, pp. 591−600.

7. Dai, H., Wang, L., Zhang, J., Liu, Y., Wang, Y., Wang, L., and Wan, X., Iron based partially pre-alloyed powders as matrix materials for diamond tools, *Powder Metall.*, 2015, vol. 58, pp. 83−86.

8. Wang, Z., Gao, K., Sun, Y., Zhang, Z., and Ren, L., Effects of bionic units in different scales on the wear behavior of bionic impregnated diamond bits, *J. Bionic Eng.*, 2016, vol. 13, no. 4, pp. 659−668.

9. Li, M., Sun, Y., Meng, Q., Wu, H., Gao, K., and Liu, B., Fabrication of Fe-based diamond composites by pressureless infiltration, *Materials*, 2016, vol. 9, p. 1006.

10. Gevorkyan, E., Mechnik, V., Bondarenko, N., Vovk, R., Lytovchenko, S., Chishkala, V., and Melnik, O., Peculiarities of obtaining diamond−(Fe−Cu−Ni−Sn) hot pressing, *Funct. Mater.*, 2017. no. 24, pp. 31−45.

11. Hou, M., Guo, S., Yang, L., Gao, J., Peng, J., Hu, T., Wang, L., and Ye, X., Fabrication of Fe−Cu matrix diamond composite by microwave hot pressing sintering, *Powder Technol.*, 2018, vol. 338, pp. 36−43.

12. Bondarenko, M.O., Mechnik, V.A., and Suprun, M.V., Shrinkage and shrinkage rate behavior in $C_{diamond}$−Fe−Cu−Ni−Sn−CrB_2 system during hot pressing of pressureless-sintered compacts, *J. Superhard Mater.*, 2009, vol. 31, no. 4, pp. 232−240.

13. Mechnik, V.A., Production of diamond−(Fe−Cu−Ni−Sn) composites with high wear resistance, *Powder Metall. Met. Ceram.*, 2014, vol. 52, nos. 9−10, pp. 577−587.

14. Borowiecka-Jamrozek, J.M., Konstanty, J., and Lachowski, J., The application of a ball-milled Fe−Cu−Ni powder mixture to fabricate sintered diamond tools, *Arch. Found. Eng.*, 2018, vol. 18, no. 1, pp. 5−8.

15. Nitkiewicz, Z. and Świerzy, M., Tin influence on diamond-metal matrix hot pressed tools for stone cutting, *J. Mater. Process. Technol.*, 2006, vol. 175, nos. 1−3, pp. 306−315.

16. Mechnik, V.A., Bondarenko, N.A., Kuzin, N.O., and Lyashenko, B.A., The role of structure formation in forming the physicomechanical properties of composites of the diamond−(Fe−Cu−Ni−Sn) system, *J. Frict. Wear*, 2016, vol. 37, no. 4, pp. 377−384.

17. Dinaharan, I., Sathiskumar, R., and Murugan, N., Effect of ceramic particulate type on microstructure and properties of copper matrix composites synthesized by friction stir processing, *J. Mater. Res. Technol.*, 2016, vol. 5, no. 4, pp. 302–316.

18. Hodge, A.M., Wang, Y.M., and Barbee, T.W., Large-scale production of nano-twinned, ultrafine-grained copper, *Mater. Sci. Eng., A*, 2006, vol. 429, nos. 1–2, pp. 272–276.

19. Levashov, E., Kurbatkina, V., and Zaytsev, A., Improved mechanical and tribological properties of metal-matrix composites dispersion-strengthened by nanoparticles, *Materials*, 2010, vol. 3, no. 1, pp. 97–109.

20. Shaw, L.L., Villegas, J., Huang, J.-Y., and Chen, S., Strengthening via deformation twinning in a nickel alloy, *Mater. Sci. Eng., A*, 2008, vol. 480, nos. 1–2, pp. 75–83.

21. Konstanty, J., *Powder Metallurgy Diamond Tools*, Amsterdam: Elsevier, 2005.

22. Uemura, M., An analysis of the catalysis of Fe, Ni, or Co on the wear of diamonds, *Tribol. Int.*, 2004, vol. 37, pp. 887–892.

23. Sidorenko, D.A., Zaitsev, A.A., Kirichenko, A.N., Levashov, E.A., Kurbatkina, V.V., Loginov, P.A., Rupasov, S.I., and Andreev, V.A., Interaction of diamond grains with nanosized alloying agents in metal–matrix composites as studied by Raman spectroscopy, *Diamond Relat. Mater.*, 2013, vol. 38, pp. 59–62.

24. Yılmaz, N.G., Goktan, R.M., and Kibici, Y., An investigation of the petrographic and physic-mechanical properties of true granites influencing diamond tool wear performance and development of a new wear index, *Wear*, 2011, vol. 271, pp. 960–969.

25. del Villar, M., Muro, P., Sánchez, J.M., Iturriza, I., and Castro, F., Consolidation of diamond tools using Cu–Co–Fe based alloys as metallic binders, *Powder Metall.*, 2001, vol. 44, pp. 82–90.

26. Li, W., Zhan, J., Wang, S., Dong, H., Li, Y., and Liu, Y., Characterizations and mechanical properties of impregnated diamond segment using Cu–Fe–Co metal matrix, *Rare Met.*, 2012, vol. 31, pp. 81–87.

27. Zhukovskii, A.N., Maistrenko, A.L., Mechnik, V.A., and Bondarenko, N.A., The stress-strain state of the bonding around the diamond grain exposed to normal and tangent loading components, Part 1: Model, *Trenie Iznos.*, 2002, vol. 23, no. 2, pp. 146–153.

28. Zhukovskii, A.N., Maistrenko, A.L., Mechnik, V.A., and Bondarenko, N.A., Stress-strain state of the matrix around the diamond grain exposed to the normal and tangent loading components, Part 2: Analysis, *Trenie Iznos.*, 2002, vol. 23, no. 4, pp. 393–396.

29. Aleksandrov, V.A., Akekseenko, N.A., and Mechnik, V.A., Study of force and energy parameters in cutting granite with diamond disc saws, *Sov. J. Superhard Mater.*, 1984, vol. 6, no. 6, pp. 46–52.

30. Aleksandrov, V.A., Zhukovskii, A.N., and Mechnik, V.A., Temperature field and wear of inhomogeneous diamond wheel at convective heat exchange, *Trenie Iznos*, 1994, vol. 15, no. 1, pp. 27–35.

31. Aleksandrov, V.A., Zhukovskii, A.N., and Mechnik, V.A., Temperature field and wear of heterogeneous diamond wheel under conditions of convectional heat transfer. Part 2, *Trenie Iznos*, 1994, vol. 15, no. 2, pp. 196–201.

32. Aleksandrov, V.A. and Mechnik, V.A., Effect of heat conduction of diamonds and heat-exchange coefficient on contact temperature and wear of cutting disks, *Trenie Iznos*, 1993, vol. 14, no. 6, pp. 1115–1117.

33. Dutka, V.A., Kolodnitskij, V.M., Zabolotnyj, S.D., Sveshnikov, I.A., and Lukash, V.A., Simulation of the temperature level in rock destruction elements of drilling bits, *Sverkhtverd. Mater.*, 2004, vol. 26, no. 2, pp. 66–73.

34. Dutka, V.A., Kolodnitskij, V.M., Mel'nichuk, O.V., and Zabolotnyj, S.D., Mathematical model for thermal processes occurring in the interaction between rock destruction elements of drilling bits and rock mass, *Sverkhtverd. Mater.*, 2005, vol. 27, no. 1, pp. 67–77.

35. Sveshnikov, I.A. and Kolodnitsky, V.N., Optimization of the hard alloy cutter arrangement in the drilling bit body, *Sverkhtverd. Mater.*, 2006, vol. 28, no. 4, pp. 70–75.

36. Franca, L.F.P., Mostofi, M., and Richard, T., Interface laws for impregnated diamond tools for a given state of wear, *Int. J. Rock Mech. Mining Sci.*, 2015, vol. 73, pp. 184–193.

37. Wang, J., Zhang, S., and Peng, F., Influence mechanism of hard brittle grits on the drilling performance of diamond bit, *J. Ann. Chim. Sci. Mater.*, 2018, vol. 42, no. 2, pp. 209–220.

38. Zhang, Z. and Chen, D.L., Consideration of Orowan strengthening effect in particulate-reinforced metal matrix nanocomposites: A model for predicting their yield strength, *Scr. Mater.*, 2006, vol. 54, no. 7, pp. 1321–1326.

39. Mechnik, V.A., Bondarenko, N.A., Dub, S.N., Kolodnitskyi, V.M., Nesterenko, Yu.V., Kuzin, N.O., Zakiev, I.M., and Gevorkyan, E.S., A study of microstructure of Fe–Cu–Ni–Sn and Fe–Cu–Ni–Sn–VN metal matrix for diamond containing composites, *Mater. Charact.*, 2018, vol. 146, pp. 209–216.

40. Mechnik, V.A., Bondarenko, N.A., Kolodnitskyi, V.M., Zakiev, V.I., Zakiev, I.M., Storchak, M., Dub, S.N., and Kuzin, N.O., Physico-mechanical and tribological properties of Fe–Cu–Ni–Sn and Fe–Cu–Ni–Sn–VN nanocomposites obtained by powder metallurgy methods, *Tribol. Ind.*, 2019, vol. 41, no. 2, pp. 188–198.

41. Mechnik, V.A., Bondarenko, N.A., Kolodnitskyi, V.M., Zakiev, V.I., Zakiev, I.M., Ignatovich, S.R., Dub, S.N., and Kuzin, N.O., Formation of Fe–Cu–Ni–Sn–VN nanocrystalline matrix by vacuum hot pressing for diamond-containing composite. Mechanical and tribological properties, *J. Superhard Mater.*, 2019, vol. 41, no 6, pp. 388–401.

42. Mechnik, V.A., Bondarenko, N.A., Kolodnitskyi, V.M., Zakiev, V.I., Zakiev, I.M., Ignatovich, S.R., Dub, S.N., and Kuzin, N.O., Effect of vacuum hot pressing temperature on the mechanical and tribological properties of the Fe−Cu−Ni−Sn−VN composites, *Powder Metall. Met. Ceram.*, 2020, vol. 58, nos. 11−12, pp. 679−691.

43. Mechnik, V.A., Bondarenko, N.A., Kuzin, N.O., and Gevorkian, E.S., Influence of the addition of vanadium nitride on the structure and specifications of a diamond−(Fe−Cu−Ni−Sn) composite system, *J. Frict. Wear*, 2018, vol. 39, no. 2, pp. 108−113.

44. Han, Y., Zhang, S., Bai, R., Zhou, H., Su, Z., Wu, J., and Wang, J., Effect of nano-vanadium nitride on microstructure and properties of sintered Fe−Cu-based diamond composites, *Int. J. Refract. Met. Hard Mater.*, 2020, vol. 91, art. 105256.

45. Mechnyk, V.A., Regularities of structure formation in diamond−Fe−Cu−Ni−Sn−CrB_2 systems, *Mater. Sci.*, 2013, vol. 49, no. 1, pp. 93−101.

46. Mechnik, V.A., Effect of hot recompaction parameters on the structure and properties of diamond−(Fe−Cu−Ni−Sn−CrB_2) composites, *Powder Metall. Met. Ceram.*, 2014, vol. 52, nos. 11−12, pp. 709−721.

47. Mechnik, V.A., Bondarenko, N.A., Kolodnitskyi, V.M., Zakiev, V.I., Zakiev, I.M., Ignatovich, S.R., and Yutskevych, S.S., Mechanical and tribological properties of Fe−Cu−Ni−Sn materials with different amounts of CrB_2 used as matrices for diamond-containing composites, *J. Superhard Mater.*, 2020, vol. 42, no. 4, pp. 251−263.

48. Kraus, W. and Nolze, G., Powder cell—a program for the representation and manipulation of crystal structures and calculation of the resulting X-ray powder patterns, *J. Appl. Cryst.*, 1996, vol. 29, pp. 301−303.

49. *Selected Powder Diffraction Data for Education Straining: Search Manual and Data Cards*, Swarthmore, PA: Int. Centre Diffraction Data, 1988.

50. Zakiev, I. and Aznakayev, E., Micro Gamma: the device for the estimation of physico-mechanical properties of materials, *J. Assoc. Lab. Autom.*, 2002, vol. 7, no. 5, pp. 44−45.

51. Storchak, M., Zakiev, I., and Träris, L., Mechanical properties of subsurface layers in the machining of the titanium alloy $Ti_{10}V_2Fe_3Al$, *J. Mech. Sci. Technol.*, 2018, vol. 32, pp. 315−322.

52. Vasil'ev, M.O., Mordyuk, B.M., Voloshko, S.M., Zakiev, V.I., Burmak, A.P., and Pefti, D.V., Hardening of surface layers of Cu−39Zn−1Pb brass at holding and high-frequency impact deformation in liquid nitrogen, *Metallofiz. Nov. Tekhnol.*, 2019, vol. 41, no 11, pp. 1499−1517.

53. Oliver, W.C. and Pharr, G.M., An improved for determining hardness and elastic modulus using load and displacement sensing indentation experiments, *J. Mater. Res.*, 1992, vol. 7, no. 6, pp. 1564−1583.

54. Firstov, S.A., Ignatovich, S.R., and Zakiev, I.M., Size effect in the micro- and nanoindentation and its compensation with regard for the specific features of initial contact, *Strength Mater.*, 2009, vol. 41, no. 2, pp. 147−155.

55. Vasylyev, M.A., Mordyuk, B.N., Sidorenko, S.I., Voloshko, S.M., Burmak, A.P., Kruhlov, I.O., and Zakiev, V.I., Characterization of ZrN coating low-temperature deposited on the preliminary Ar^+ ions treated 2024 Al-alloy, *Surf. Coat. Technol.*, 2019, vol. 361, pp. 413−424.

56. Zakiev, V., Markovsky, A., Aznakayev, E., Zakiev, I., and Gursky, E., Micro-mechanical properties of bio-materials, *Proc. SPIE*, 2005, vol. 5959.

57. Okipnyi, I.B., Maruschak, P.O., Zakiev, V.I., and Mocharskyi, V.S., Fracture mechanism analysis of the heat-resistant steel 15Kh2MFA(II) after laser shock-wave processing, *J. Failure Anal. Prev.*, 2014, vol. 14, no. 5, pp. 668−674.

58. Zakiev, I., Gogotsi, G.A., Storchak, M., and Zakiev, V., Glass fracture during micro-scratching, *Surfaces*, 2020, vol. 3, pp. 211−224.

59. Fuertes, V., Cabrera, M.J., Seores, J., Muñoz, D., Fernández, J.F., and Enríquez, E., Enhanced wear resistance of engineered glass-ceramic by nanostructured self-lubrication, *Mater. Des.*, 2019, vol. 168, art. 107623.

60. *ASTM G99-17: Standard Test Method for Wear Testing with a Pin-on-Disk Apparatus*, West Conshohocken, PA: ASTM Int., 2017.

61. *ASTM G171-03: Standard Test Method for Scratch Hardness of Materials Using a Diamond Stylus*, West Conshohocken, PA: ASTM Int., 2017.

62. Kovalchenko, A.M., Goel, S., Zakiev, I.M., Pashchenko, E.A., and Al-Sayegh, R., Suppressing scratch-induced brittle fracture in silicon by geometric design modification of the abrasive grits, *J. Mater. Res. Technol.*, 2019, vol. 8, no. 1, pp. 703−712.

Translated by O. Zhukova